Article

Quantum stochastic resonance in a single-photon emitter

Check for updates

H. Mannel [1,4] ✉, J. Zöllner [1,4], E. Kleinherbers[2], M. Zöllner[1], N. Schwarz[1], F. Rimek[1], A. D. Wieck [3], A. Ludwig [3], A. Lorke [1], J. König [1] & M. Geller[1]

Stochastic resonance is a phenomenon in which fluctuations enhance an otherwise weak signal. It has been found in many different systems in paleoclimatology, biology, medicine, and physics. The classical stochastic resonance due to thermal noise has recently been experimentally extended to the quantum regime, where the fundamental randomness of individual quantum events provides the noise source. Here, we demonstrate quantum stochastic resonance in the single-electron tunneling dynamics of a periodically driven single-photon emitter, consisting of a self-assembled quantum dot that is tunnel-coupled to an electron reservoir. Such highly-controllable quantum emitters are promising candidates for future applications in quantum information technologies. We monitor the charge dynamics by resonant optical excitation and identify quantum stochastic resonance with the help of full counting statistics of tunneling events in terms of the Fano factor and extend the statistical evaluation to factorial cumulants to gain a deeper understanding of this far-reaching phenomenon.

Noise is usually a nuisance for any measurement as it superimposes and thereby masks the signal one wants to measure. There are, however, also scenarios in which noise plays an integral role in the system dynamics. This includes the phenomenon of stochastic resonance[1–3], in which fluctuations enhance an otherwise weak signal. The effect has been observed in a wide range of different systems, including the periodicity of ice ages[4], biological signal processing[5–7] and machine learning[8].

The paradigmatic model exhibiting stochastic resonance consists of a driven bistable system, in which the energy difference between the two states is modulated in time. A potential barrier that is much higher than the driving amplitude prevents the switch between the two states. Adding fluctuations due to thermal noise allows for thermal activation over the barrier, and the system can switch between the two states to follow the external drive. The response of the system to the external drive is thus enhanced by the noise. With increasing noise, the measurement signal becomes more pronounced until, for large fluctuations, the switching of the bistable system becomes independent of the external driving. This results in a stochastic resonance of the measurement signal, indicated by a large signal-to-noise ratio at the resonance frequency f_{res}.

About 30 years ago, a quantum version of the stochastic resonance has been theoretically predicted[9–12]. It relies on the fact that even in the absence of thermal fluctuations, stochastic resonance is possible due to quantum noise. The latter is generated by the inherent phenomenon of quantum tunneling through the potential barrier. The required ingredients are quite generic and, therefore, quantum stochastic resonance has been predicted to appear in different systems from general bistable double well potentials[9–15] and specific systems like arrays of superconducting qubits[16], photoionization of an atom with femtosecond pulses[17] and in nuclear magnetic resonance experiments on water[18]. However, very few experiments have demonstrated the effect so far. It has been found in electrostatically defined quantum dots[19], where switching between two charge states is due to electron tunneling between the quantum dot and an electron reservoir. Quantum stochastic resonance has also been found in a single Fe atom placed on a Cu_2N substrate and contacted by a spin-polarized tip of a scanning tunneling microscope[20]. Here, and in both prior works on quantum stochastic resonance, the noise in the system is fixed as it is given by the stochastic process of electron tunneling and the modulation frequency is changed. The Fano factor is used as a measure of the signal-to-noise ratio.

In this work, we report on the observation of quantum stochastic resonance in a highly controllable single-photon emitter heterostructure consisting of (i) a single self-assembled InAs/GaAs quantum dot (QD) and (ii) an electron reservoir to charge and discharge the dot. Quantum stochastic resonance is identified as the synchronization of electron tunneling between dot and reservoir driven by periodic modulation of the gate voltage while monitoring the charge state with high-resolution resonance fluorescence[21–26] in real-time[27–29]. Since single-photon emitters can act as spin-photon interfaces[30–32] in future quantum networks[33,34], our findings could serve as a first step towards regulation of photon streams in

continuous-wave laser excitation combined with an external electrical drive. Furthermore we improve the quantitative understanding of quantum stochastic resonance in general. We introduce normalized factorial cumulants of the full counting statistics as a theoretical tool, which allows us to shed light on the non-trivial question of the exact conditions for this quantum-mechanically driven resonance phenomenon.

Results and discussion
Charge dynamics in a driven quantum dot
Real-time charge detection. A schematic illustration of our sample structure and experimental setup is shown in Fig. 1a. A self-assembled InAs/GaAs dot is embedded in a p-i-n diode structure for electrical control (details in methods section and in supplementary note 1) and cooled in a bath cryostat to 4.2 K[35]. The dot is charged and discharged by tunneling of electrons from or to an electron reservoir, i.e., a highly doped GaAs layer below the dot. A gate voltage V_g allows us to tune the occupation probability of the QD from zero to one, as the lowest electron state is energetically shifted through the Fermi edge of the electron reservoir (see upper insets in Fig. 1b). The charge state is detected in real-time by means of resonance fluorescence from the neutral exciton transition[28].

We use the dark-field technique (crossed excitation-collection polarization) to separate the reflected laser light from the QD signal[36–39]. The light emitted from the QD is detected by an avalanche photo diode (APD) that serves as a single-photon detector (see methods section). The detected photons are accumulated over a binning time t_{bin} to obtain a measure of the fluorescence brightness[40].

Figure 1b shows the resonance fluorescence (RF) of the exciton transition (X^0) with its fine-structure splitting[41,42] as a function of gate voltage V_g and laser frequency. Due to the quantum confined-Stark effect, the applied gate voltage shifts the frequency of the exciton resonance towards higher energies as the gate voltage is increased. In addition, the energy of the quantum dot states will decrease with respect to the chemical potential μ of the electron reservoir until, around $V_g = 0.5$ V, an electron can tunnel into the s-state of the dot, marked by the dashed line in Fig. 1b and schematically illustrated by the inset in the upper right corner. This shifts the optical resonance, and the neutral exciton transition vanishes. Close to this gate voltage, the QD charge fluctuates in time and the exciton transition can be used as a sensitive optical detector to observe all tunneling events in real-time.

The gate voltage range between the QD being uncharged and charged is given by the reservoir temperature of 4.2 K and a gate-voltage-to-energy conversion factor ('lever arm') of 15.2 mVmeV^{-1}. This is demonstrated in Fig. 2a, which displays the tunneling rates γ_{In} and γ_{Out} for tunneling into and out of the QD, that were determined by means of the pulsed measurement scheme presented in refs. 25,43. For $V_g < 0.47$ V, γ_{In} vanishes and the QD is mostly empty, while for $V_g > 0.52$ V, γ_{Out} vanishes, and the QD becomes occupied with a single electron. In between, the average QD occupation, given by $\gamma_{In}/(\gamma_{In} + \gamma_{Out})$, changes continuously from 0 to 1 with increasing gate voltage. The energetic position of the QD state with respect to the chemical potential μ of the electron reservoir is shown in three schematic insets. At $V_g = 494$ mV, the tunneling rates γ_{In} and γ_{Out} are approximately equal, with electrons randomly tunneling back and forth between the QD and reservoir. Note that here no Auger process is possible because only the exciton (and not the trion) transition is driven. A charged QD yields a low ("off") fluorescence signal while the uncharged dot leads to a bright ("on") fluorescence signal. The result is a random telegraph signal in the optical response of the QD[28].

To drive the system, we modulate the gate voltage with a square function, as shown at the bottom of Fig. 2b and also indicated by the modulation scale bars in Fig. 2a. Stochastic resonance can be qualitatively characterized by the switching behavior of the charge state: the switching becomes more regular at resonance while it is dominated by fluctuations away from it.

In Fig. 2b, a photon stream without modulation is shown, where the electron tunnels in and out randomly. With a modulation amplitude of

16 mV, though, even the unaided eye can discern that the low/high value of the gate voltage (white/grey region in Fig. 2b) is predominantly accompanied with a large/small RF signal in the telegraph stream. Hence, the charge switching is synchronized with the driving voltage, indicating stochastic resonance.

Full counting statistics. In Fig. 2b, center, the synchronization between voltage drive and charge-state switching is evident. A systematic analysis of quantum stochastic resonance, however, requires a quantitative tool not only to characterize how regular the switching occurs but also to identify the resonance condition, i.e. to find (for given gate voltage values) the modulation frequency f_{mod} for which the switching is most regular. For this, a statistical analysis of the switching behavior needs to be performed.

To address the switching dynamics, we make use of the framework of full counting statistics, applied to the number of switching events within a given time span. The central quantity is the probability distribution $P_N(\Delta t)$ that N switching events have taken place within an interval of length Δt. To be specific, we decide to count only tunneling-out events. The alternative choices of counting only tunneling-in events or counting both types of tunneling events (as it was done in ref. 19) would render our conclusions about the stochastic resonance unchanged. An example for the distribution $P_N(5\ \text{ms})$ for a modulation amplitude of 16 mV and frequency of $f_{mod} = 796$ Hz is shown in Fig. 3. The distribution $P_N(5\ \text{ms})$ (red dots) is broadened as compared to a completely regular behavior of one tunneling-out event per modulation cycle (gray). This reflects the stochastic nature of tunneling. The measured distribution is, however, much sharper than a Poisson distribution with the same mean value (blue line). The latter would be expected if all tunneling-out events were independent of each other. The reduced width of the measured distribution, thus, indicates that the switching behavior has become more regular. We remark that this is not yet a unique indicator of stochastic resonance, since even in the undriven system correlations (due to Pauli exclusion and electron-electron interactions) lead to sub-Poissonian statistics.

A more quantitative comparison of a given distribution, within the completely random and completely regular limits, also used by previous experimental studies[19,20], is provided by the signal-to-noise ratio or its inverse, the Fano factor

$$F = \frac{\langle N^2 \rangle - \langle N \rangle^2}{\langle N \rangle}, \qquad (1)$$

i.e. the ratio of the variance $\sigma^2 = \langle N^2 \rangle - \langle N \rangle^2$ and the mean value $\lambda = \langle N \rangle$ for the number N of measured switching events. If the tunneling-out events occurred completely independent of each other, the full counting statistics would be Poissonian, which implies a Fano factor of 1. However, correlations are always present since after a tunneling-out event an electron has to tunnel in before the next tuneling-out can occur. For the undriven case, the Fano factor is known[44–48] to be $F = \frac{\gamma_{In}^2 + \gamma_{Out}^2}{(\gamma_{In} + \gamma_{Out})^2}$, which ranges between values of $F = 1$ for $\gamma_{In} \ll \gamma_{Out}$ or $\gamma_{Out} \ll \gamma_{In}$ and $F = 0.5$ for $\gamma_{In} = \gamma_{Out}$. The measured value of $F = 0.35$ in Fig. 4, therefore, indicates a more regular switching behavior in the presence of driving. In the limit of completely regular switching, the Fano factor would be $F = 0$. With this tool at hand, stochastic resonance can be defined by the minimum of F as a function of the driving frequency for fixed switching rates or as a function of switching rates for fixed driving frequency[19].

The characterization of such a complex process as quantum stochastic resonance, using only two numbers λ and σ^2, however, seems to be limited. Deeper insight is expected from a more complete theoretical evaluation. As one possibility, the spectral properties of the noise, expressed in terms of a frequency-dependent Fano factor, has been employed for the analysis of the quantum stochastic resonance[49]. Here, we suggest an alternative route that is based on the idea that a distribution function can be completely characterized in terms of cumulants. The mean value λ and the variance σ^2 are nothing but the first- and second-order ordinary cumulants. They are
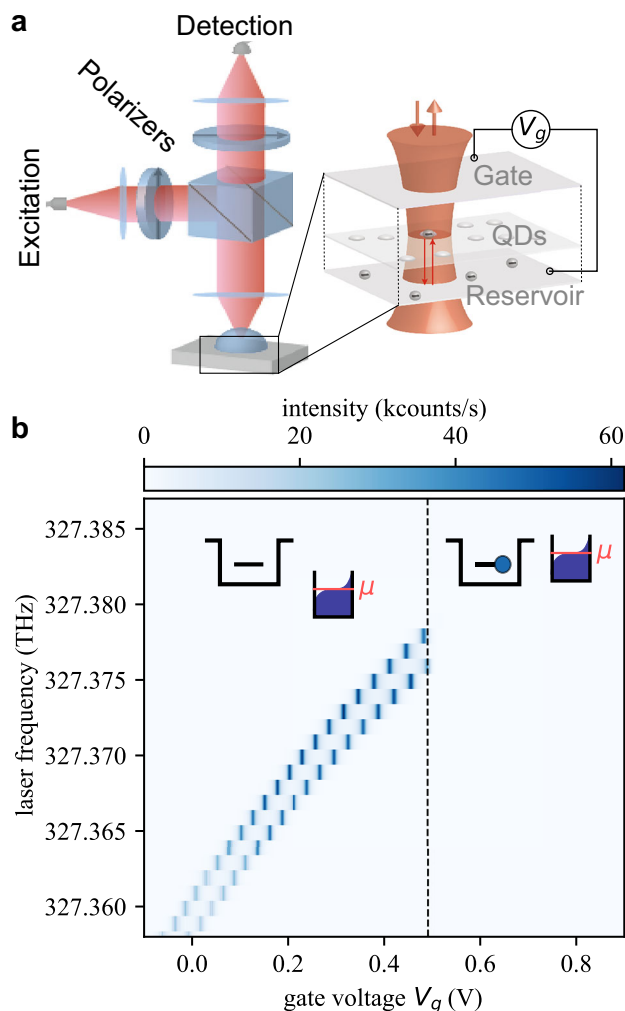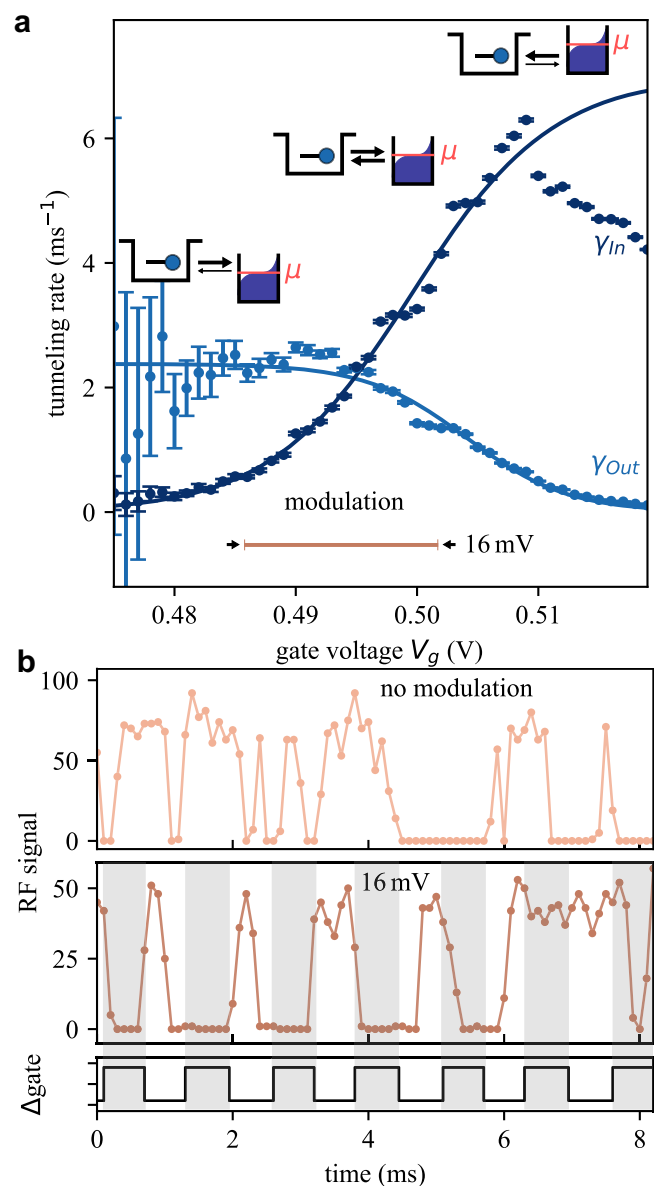
Fig. 1 | Resonance fluorescence in a single quantum dot. a The excitation laser is reflected onto the sample by a 90:10 beamsplitter. Two crossed polarisers are used to suppress the reflected laser light. The QDs are embedded in a p-i-n-diode structure between a gate electrode at the top and an electron reservoir at the bottom of the structure. A gate voltage V_g can be applied to control the QD charge state and its transition energies. **b** Exciton transition X^0 as a function of the laser excitation frequency and applied gate voltage. At a gate voltage of $V_g = 0.5$ V, the QD is charged with an electron from the reservoir and the X^0 transition can no longer be excited by the resonant laser. The insets show schematically the two situations around the transition voltage at $V_g = 0.5$ V, where the chemical potential μ is below (left inset) and above (right inset) of the lowest quantum dot state.

Fig. 2 | The electron dynamics, revealed in the optical resonance fluorescence signal. a Electron tunneling rates γ_{In} and γ_{Out} as a function of the gate voltage V_g. Solid lines are fits to the data, given by the Fermi-distribution in the electron reservoir. The insets illustrate the continuous increase of γ_{In} with increasing gate voltage, while γ_{Out} decreases with increasing chemical potential with respect to the QD level. Around the gate voltage where both rates are equal, the voltage modulation for the quantum stochastic resonance takes place. The error bars are derived via R^2 of the exponential fit presented in ref. 43. **b** Telegraph signals with a binning of 100 μs, showing the single electron tunneling events between the quantum dot and the reservoir as a switching on and off of the resonance fluorescence signal. For no modulation the electron tunnels in and out randomly with fixed rates γ_{In} and γ_{Out}. When the modulation of the gate voltage is on, correlations start to occur between the electron tunneling and V_g. This is shown with shaded areas as a guide to the eye where a switching event should occur for deterministic transport. The amplitude of the a. c. drive is indicated as a scale bar in **a**.

sufficient to fully describe a Gauss distribution. Deviations from a Gauss distribution are expressed in terms of third- and higher-order ordinary cumulants. They have been measured in quantum-dot systems[50–52] up to 20-th order. Our aim, however, is to measure deviations from a Poisson rather than a Gauss distribution. Therefore, we make use of factorial cumulants[53–58], which are better suited for discrete rather than continuous stochastic variables. They prevent unwanted universal oscillations[51,52] and are resilient against detector imperfections[59]. They have proven successful in determining the rates for spin relaxation[28] as well as Auger recombination and spin-flip Raman scattering[60] from random telegraph signals such as the ones investigated here.

The factorial cumulants $C_{F,m}$ of order m can be calculated using the generating function

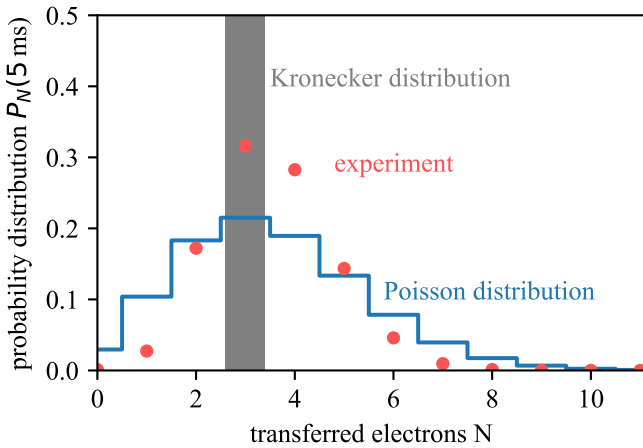$$S_F(z) = \ln \sum_N z^N P_N, \qquad (2)$$

i.e., the logarithm of the z-transform of the probability distribution P_N, and taking their derivatives with respect to the counting variable z,

$$C_{F,m} = \left[\partial_z^m S_F(z) \right]\big|_{z=1}. \qquad (3)$$

Explicit expressions for the first four factorial cumulants in terms of moments $\langle N^m \rangle$ are given in Eqs. (S2a-d), see supplementary note 5.

Fig. 3 | Probability distribution of electron transport. Probability distribution $P_N(\Delta t = 5$ ms) (red dots) for the number of electrons transferred at a modulation frequency of $f_{mod} = 796$ Hz with amplitude 16 mV. The experimental data is compared to a Kronecker distribution (gray), corresponding to completely regular switching, and a Poisson distribution (blue line) as a completely uncorrelated transport. The measured distribution is narrower than a Poisson distribution for the same mean value. The reduced width of a distribution indicates a more regular electron transport.

Using the factorial cumulants, the Fano factor can be alternatively expressed as

$$F = 1 + \frac{C_{F,2}}{C_{F,1}} , \qquad (4)$$

where the first-order factorial cumulant $C_{F,1} = \langle N \rangle = \lambda$ is the mean value of counts. Higher-order factorial cumulants vanish for a Poisson distribution of completely uncorrelated discrete events, $C_{F,m}^{Poisson} = 0$ for $m \geq 2$. In the opposite limit of fully regular switching behavior, the distribution is described by a Kronecker delta, $P_N^\delta = \delta_{N,\lambda}$ which yields $C_{F,m}^\delta = (-1)^{(m-1)}(m-1)!\lambda$.

For a quantitative measure of the regularity of the switching behavior, it is useful to normalize the measured factorial cumulants $C_{F,m}$ with $C_{F,m}^\delta$. We, thus, define for $m \geq 2$ the normalized factorial cumulants

$$x_m := \frac{(-1)^{m-1} C_{F,m}}{(m-1)! C_{F,1}} , \qquad (5)$$

that are all 0 for a Poisson and 1 for a Kronecker distribution.

To infer the factorial cumulants (and Fano factor) from the measured random telegraph stream of 15 min for a given time interval length Δt, we first determine the probability distribution $P_N(\Delta t)$ for the number N of tunneling events. Then, we calculate the moments $\langle N^m \rangle$ up to $m = 4$ and insert them into Eq. (1) for the Fano factor and Eqs. (S2a-d) shown in supplementary note 5 for the factorial cumulants, respectively.

Quantum stochastic resonance
Having established that normalized factorial cumulants x_m provide a quantitative measure how regular or random a process is, we define the quantum stochastic resonance frequency as the frequency that maximizes x_m. We will show below that the frequency that maximises x_m depends on the order m of the chosen factorial cumulant, raising the question of how rigorous a resonance frequency can be defined in the context of stochastic resonance.

Fano factor. We begin with a discussion of x_2. It is related to the Fano factor by $F = 1 - x_2$, i.e. a maximum in x_2 is equivalent to a minimum in F. In the field of quantum optics, $-x_2 = C_{F,2}/C_{F,1} =: Q$ is also known as the
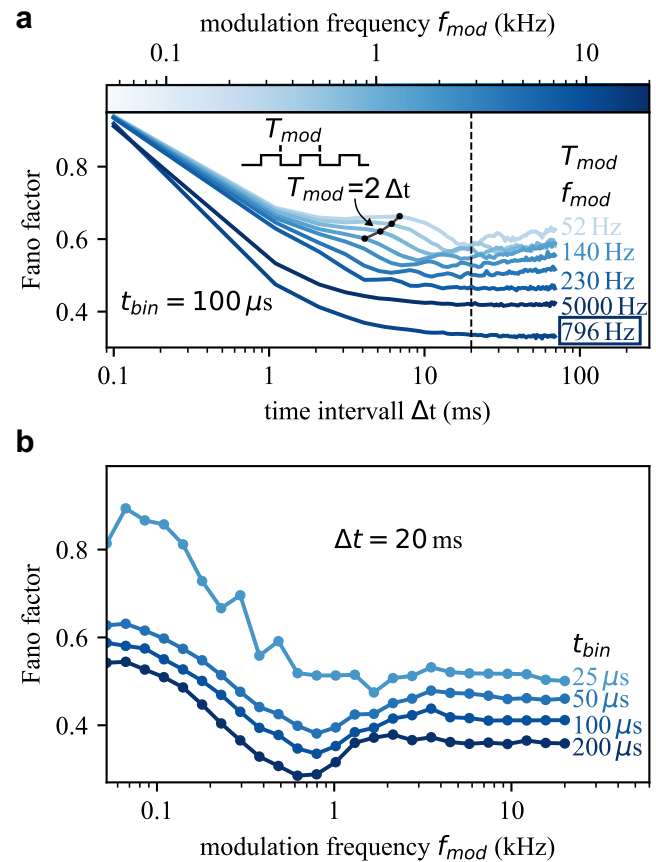
Fig. 4 | Time evolution of the Fano factor. a The Fano factor versus the time interval Δt for selected modulation frequencies from 52 Hz (light blue) to 5 kHz (dark blue) and a modulation amplitude of 16 mV. At a driving frequency of 796 Hz, the Fano factor is at a minimum for all Δt, indicating stochastic resonance around this frequency. The dashed line is at the time interval of $\Delta t = 20$ ms, where we define the long time limit (see subsection Fano factor). The maxima of the Fano factor marked with black dots are artefacts that occur when the time interval Δt is half of the modulation period T_{mod}; schematically shown in the inset and explained in more detail in the main text. **b** The long time limit of the Fano factor for different binning times t_{bin} of the single photon stream. The decrease in the Fano factor at ≈ 800 Hz is due to the quantum stochastic resonance.

Mandel Q-parameter to characterize deviations from Poissonian photon statistics[61].

The distribution $P_N(\Delta t)$ depends on the length Δt of the time interval in which the tunneling-out events are counted. Furthermore, the accuracy with which the random telegraph signal reflects the actual charge switching of the system depends on the binning time t_{bin}, which is the time interval used to group the photon arrival events. The binning time t_{bin} is chosen large enough to distinguish the charged from the uncharged state by a clear separation of the two peaks in the histogram of the RF counts per bin, see Fig. S2 in supplementary note 2. Both times, Δt and t_{bin}, can be chosen a posteriori from the measured stream of individual photon counts[40]. They introduce two new time scales that are unrelated to stochastic resonance. We must therefore optimize them in our quest for stochastic resonance to avoid artifacts.

In Fig. 4a, we show the Fano factor as a function of Δt for different modulation frequencies ranging from 52 Hz up to 5 kHz. For all data sets that each comprise a time span of 15 min, we used a modulation amplitude of 16 mV and a binning time of $t_{bin} = 100$ μs. Each data set contains 600k events on average. For very short intervals Δt, most intervals accommodate no or, with a small probability, only one tunneling-out event. This can be described by a Bernoulli distribution $P_N^{Bernoulli} = (1-q)\delta_{N,0} + q\delta_{N,1}$ with $0 \leq q \ll 1$, for which the Fano factor $F = 1 - q$ approaches the Poissonian

Fig. 5 | Quantum stochastic resonance indicated by the Fano factor. a Fano factor as a function of the modulation frequency for different modulation amplitudes (data points) compared with theoretical model curves (solid blue lines). The model has no fitting parameters. The modulation is symmetrical around $V_g = 496$ mV, where $\gamma_{In} = \gamma_{Out}$. The minimum around ≈ 800 Hz is due to quantum stochastic resonance. The dashed vertical line is given by Eq. (6) for a 1 mV modulation. **b** The Fano factor as a function of the modulation frequency for 16 mV and 87 mV. The exact values of the upper, lower and average value of the gate voltage are given in Table S1 in supplementary note 3. The vertical lines are given by Eq. (7) for a 16 mV and 87 mV modulation.
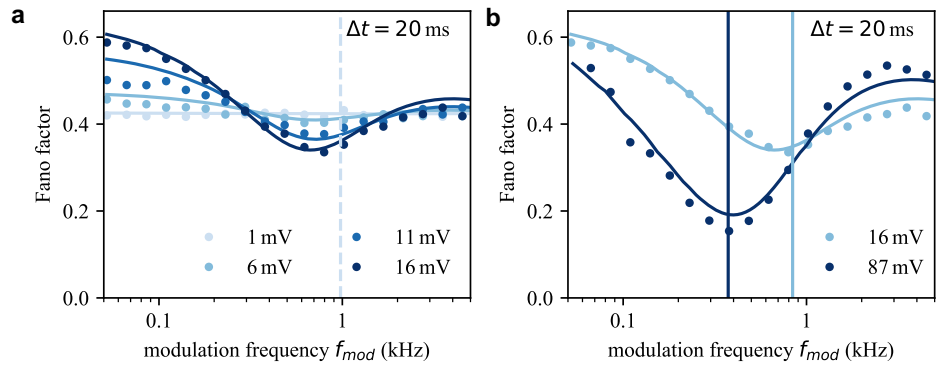
value $F \to 1$ for $\Delta t \to 0$ (which implies $q \to 0$). As a result, operating in the short-time limit is inappropriate for unraveling quantum stochastic resonance. Instead, it is advantageous to go to the long-time limit, in which each interval contains many counts of tunneling-out events such that the Fano factor becomes independent of Δt. In the following, we choose $\Delta t = 20$ ms (indicated by the vertical dashed line in Fig. 4a) to ensure that, on the one hand, the long-time limit is already reached and that, on the other hand, slow, long-term fluctuation in the experimental setup will not become relevant yet.

Since the period $T_{mod} = 1/f_{mod}$ of the gate modulation already introduces a time scale, one may be tempted to choose this time scale for Δt as well. This, however, may introduce artifacts as shown in Fig. 4a, where the choice $\Delta t = T_{mod}/2$ is indicated by black dots. We find that, at least for low frequencies, the Fano factor is enhanced around this choice of Δt. To identify quantum stochastic resonance, we vary the modulation frequency f_{mod}. Fig. 4a shows that for all values of Δt the Fano factor first decreases with increasing modulation frequency (from $f_{mod} = 52$ Hz to $f_{mod} = 796$ Hz), and subsequently increases when the modulation frequency is set to 5 kHz (or larger). This is shown more clearly in Fig. 4b, which depicts the Fano factor as a function of the modulation frequency f_{mod} for different values of the binning time t_{bin}. The interval length is fixed at the long-time limit of $\Delta t = 20$ ms. For a binning time of $t_{bin} = 100$ µs, as chosen in Fig. 4a, the Fano factor has a minimum at $f_{mod} = 796$ Hz.

The binning time t_{bin} affects the accuracy of the charge-state switching detection. A short binning time provides high time resolution, however, increases noise, leading to false event detection. This explains why at $t_{bin} = 25$ µs, the Fano factor shows no clear minimum. Increasing t_{bin} reduces false detections. However, this comes at the expense of time resolution, which results in fast events being missed. At $t_{bin} = 200$ µs, the Fano factor shows a clear minimum, however, slightly shifted. As a compromise, we choose $t_{bin} = 100$ µs, the smallest value where the resonance remains well pronounced.

In Fig. 5a and b, we show the Fano factor as a function of the modulation frequency for five different modulation amplitudes. In all cases, the average gate voltage is chosen close to the value where the in- and out-tunneling rates are equal to each other (the exact values of the upper, lower and average value of the gate voltage is given in Table S1 in supplementary note 3). A modulation amplitude of 1 mV is not sufficient to identify stochastic resonance. With increasing amplitude, however, a pronounced minimum develops around $f_{mod} \approx 800$ Hz. For a modulation amplitude of 16 mV, the Fano factor drops below 0.35, see Fig. 5a.

In Fig. 5b, we compare the Fano-factor for a moderate modulation amplitude (16 mV) to that for a high amplitude (87 mV). For the high amplitude, we not only observe a deep minimum, down to $F = 0.15$. We also find that the position of the stochastic resonance is strongly shifted towards a lower frequency of about 500 Hz, which is discussed in the next section. We note an experimental detail here: Due to the larger modulation amplitude, the laser is no longer in resonance with the exciton X^0 transition (see Fig. 2a) during the half cycle with the larger gate voltage. As a result, the electron

dynamics by photon counting is only detected during the lower gate voltage phase.

For all voltage amplitudes, we compare the measured data (dots) with a theoretical model (lines) that takes the finite time resolution of the detector into account, see Methods. We find that both the position and the depth of the minimum are well reproduced, see Fig. 5. Missed events due to the finite time resolution of the detector reduce the measured $C_{F,1}$ while $C_{F,2}$ remains almost unaffected due to the resilience of the higher-order factorial cumulants against detector imperfections[59]. This decreases the Fano factor but hardly moves the position of the minimum.

Resonance frequency. The value of the resonance frequency $f_{res} = 1/T_{res}$ depends in a complicated way on all four rates $\gamma_{In,low}$, $\gamma_{In,high}$, $\gamma_{Out,low}$ and $\gamma_{Out,high}$, where $\gamma_{In,low/high}$ is the rate for charging the quantum dot during the low/high value of the gate voltage and, similarly $\gamma_{Out,low/high}$, the rate for discharging. There are, however, two limits in which simple analytical expressions can be derived (shown in Fig. 5 as vertical lines). To achieve this, we compare the modulation period $T_{mod} = 1/f_{mod}$ with the waiting times for the quantum dot being in a given state before it switches, i.e., the inverse of the corresponding rate.

For small modulation amplitudes, i.e. in the linear-response regime, we find the condition for stochastic resonance by requiring that there is exactly one tunneling-out event (and, therefore, also one tunneling-in event) per modulation cycle. For this, the modulation period T_{mod} has to be equal to the sum of the waiting times of the quantum dot to be charged and discharged, respectively, where we can use the tunneling rates γ_{In} and γ_{Out} of the undriven system and find[62]

$$T_{res} = \frac{1}{\gamma_{In}} + \frac{1}{\gamma_{Out}} \qquad (6)$$

since γ_{In}^{-1} is the waiting time for the QD being uncharged and γ_{Out}^{-1} for being charged. For the present experiment with $\gamma_{In} = \gamma_{Out} =: \gamma$, this reduces to the condition $2f_{res} = \gamma$[63]. The value of this estimate for a modulation amplitude of 1 mV, where stochastic resonance is not yet visible, is shown as a dashed line in Fig. 5a. Already for 6 mV modulation amplitude, the linear-response estimate can no longer be used since the low- and high-voltage tunneling rates strongly differ from each other (and therefore also from the undriven case).

A simple analytic expression can also be found in the regime $\gamma_{In,low} \ll \gamma_{Out,low}$ and $\gamma_{Out,high} \ll \gamma_{In,high}$, for which a large modulation amplitude is necessary (but not sufficient). In the extreme limit of $\gamma_{In,low} = 0$ and $\gamma_{Out,high} = 0$, a perfectly regular switching behavior with exactly one discharging event per cycle is achieved in the limit $T_{mod} \to \infty$. This implies (for $\Delta t = T_{mod}$) a vanishing Fano factor in the limit $f_{mod} \to 0$ and, thus, qualitatively explains why the minimum of the Fano factor is shifted towards lower frequencies for large modulation amplitudes. For small but finite $\gamma_{In,low}$ and $\gamma_{Out,high}$, the regular switching behavior is destroyed once the quantum dot can be charged during the low-voltage ($T_{mod}/2 = \gamma_{In,low}^{-1}$)

a

b
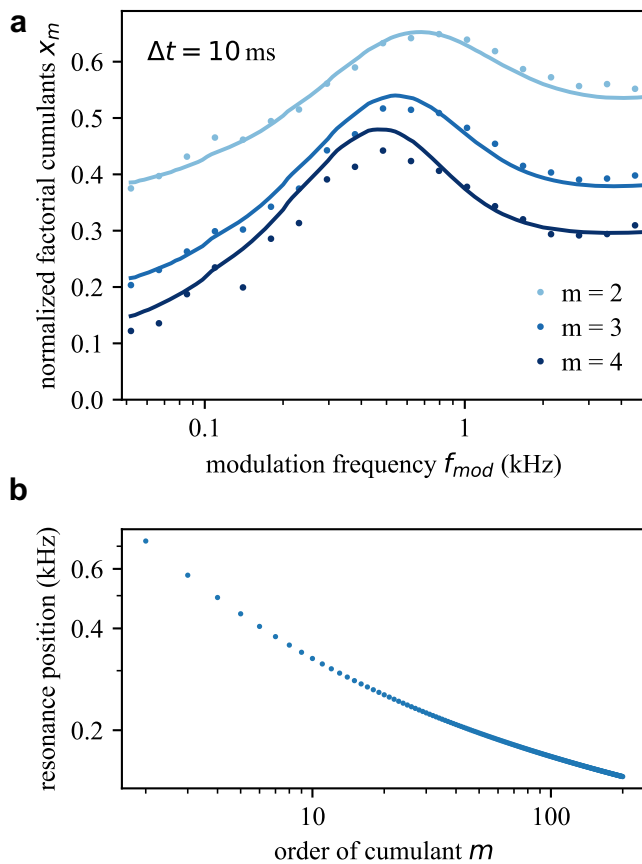
Fig. 6 | Quantum stochastic resonance indicated by factorial cumulants. a The second, third and fourth normalized factorial cumulant x_m as a function of the modulation frequency for the experimental data as blue dots and the model as solid blue lines at a modulation amplitude of 16 mV and a time interval length of $\Delta t = 10$ ms. A value of $x_m = 1$ would indicate completely regular and $x_m = 0$ completely random switching, respectively. A resonance can be seen at around 800 Hz, shifting towards lower modulation frequencies with higher order of the cumulant. **b** The modeled resonance frequency f_{res} as a function of the cumulant order for an ideal detector. Note how f_{res} decreases towards zero with increasing order and no longer satisfies the simple relation $2f_{res} = \gamma$ (see Eq. (6)).

or discharged during the high-voltage phase ($T_{mod}/2 = \gamma_{Out,high}^{-1}$). Taking the smaller of the two modulation periods and reducing the modulation period by a factor 1/2 to ensure that the destruction of the regular switching behavior has not yet set in, we arrive at

$$T_{res} = \frac{1}{\max\{\gamma_{In,low}; \gamma_{Out,high}\}}, \tag{7}$$

i.e. the larger of the two small rates determines the resonance condition. The vertical lines in Fig. 5b demonstrate a good agreement of the estimate with the measured data.

Higher-order factorial cumulants

Going beyond the second-order normalized factorial cumulant x_2 (or equivalently the Fano factor or the Mandel Q-parameter), we now also consider the higher-order terms x_3 and x_4 as a function of the modulation frequency f_{mod}. This is shown in Fig. 6a for 16 mV modulation amplitude and a time interval length of $\Delta t = 10$ ms. We find good agreement between experimental data (dots) and theoretical model (lines) without any fitting parameter. In each order m, we find a clear resonance. This nicely shows that the influence of stochastic resonance affects the statistical distribution far beyond the second moment or the Fano factor.

We find that the resonance frequency decreases with increasing order m. While experimentally we can only access the first few orders (Fig. 6a), we can calculate them within our theoretical model up to very high order, see Fig. 6b, and find a pronounced shift with no obvious lower bound. A physical understanding of this intriguing behavior remains an open question. It demonstrates, however, that the intuitive assessment that stochastic resonance occurs at the frequency given by the switching rate is incomplete.

Finally, we remark that higher-order ordinary cumulants are not useful for identifying stochastic resonance. They vanish ($C_m = 0$ for $m \geq 2$) for a Kronecker distribution ($P_N^\delta = \delta_{N,\lambda}$), but these zeroes of C_m as a function of the frequency are masked by trivial zeroes that arise due to universal oscillations[51], see supplementary note 9.

Conclusions

In conclusion, we have demonstrated quantum stochastic resonance in the dynamics of single-electron tunneling of a periodically driven two-state quantum system which consists of an electron reservoir and a quantized state in a single quantum emitter. The tunneling events are detected in real-time using resonance fluorescence on the exciton transition as an optical readout scheme. The telegraph signal of the tunneling events allows us to analyze the quantum stochastic resonance using full counting statistics. Quantum stochastic resonance is indicated by a dip in the Fano factor as well as a peak in the normalized factorial cumulants as a function of the driving frequency. We discuss the dependence of the resonance frequency on the modulation amplitude and find simple expressions both for linear response and the limit of strong nonequilibrium. Furthermore, we find a shift of the resonance frequency as a function of the order of the factorial cumulants. This shows that the question about the exact condition for stochastic resonance is non-trivial, and we expect that our study will trigger further investigations about the origin as well as the qualitative and quantitative description of quantum stochastic resonance. We advocate to apply normalized factorial cumulants for a quantitative analysis of quantum stochastic resonance in other devices as well.

Methods

QD sample structure

The sample is grown by molecular beam epitaxy and contains a single layer of self-assembled InAs/GaAs quantum dots (QDs) embedded within a GaAs matrix. The QDs are incorporated into a p-i-n-diode structure for precise charge state control (see supplementary note 1). The n-doping of the diode serves as a three-dimensional electron reservoir (back gate), allowing controlled charging of the QD or setting it to a regime where an electron can tunnel in and out of the QD by adjusting the gate voltage V_g and the shift of QD exciton energy levels through the quantum-confined Stark effect. To enhance collection efficiency within the spectral range, the sample includes a Bragg reflector of GaAs/AlGaAs layers. Moreover, the photon collection efficiency is improved by a zirconia solid immersion lens on top of the sample.

Resonance fluorescence measurement technique

We use resonance fluorescence to optically detect the charge state of the QD, which is achieved using a confocal microscopy setup with a 90:10 beam splitter head and a sample mounted in a helium bath cryostat at 4.2 K. The resonant excitation and the detection of the scattered light from the laser and QD pass along the same path through a 0.68 NA objective lens. To suppress the scattered laser light from the QD photons, we use the standard cross-polarization technique, where two linear polarizers before and after the beam-splitter suppress the laser light by at least a factor of 10^7. The photons are detected by a single photon detector (an avalanche photo diode), and we achieve a laser-background-to-QD-signal ratio well below 1%. With the particular QD investigated here, a maximum photon count rate of 4 MCounts/s (2 MCounts/s per fine-structure splitted exciton transition) was achieved.

Post processing of the photon stream

Single photons are detected using an APD and time-correlation with a time-to-digital converter, generating a list of arrival times for each photon-counting event. The telegraph signal of the electron tunneling events is derived by counting the number of photon events within a selected binning time t_{bin}. The time resolution of the photon stream can be adjusted after the actual measurement. Post processing enables us to find an optimal binning time that achieves the highest possible bandwidth while still distinguishing the excitonic on- and off-state of the QD[40] (see supplementary note 2).

Theoretical Model

To calculate the factorial cumulants, we first introduce the state-resolved probability distribution $P_{\chi,N}(t)$ for the two charge states $\chi = 0, 1$, defined as the combined probability that at time t the quantum dot is in charge state χ and N tunneling-out events have occurred since the beginning of counting at time t_0. Their z-transforms $P_{\chi,z} := \sum_N z^N P_{\chi,N}$ are governed by the master equation[55,56,59]

$$
\begin{aligned}
\dot{P}_{0,z}(t) &= -\gamma_{In}(t)P_{0,z}(t) + z\gamma_{Out}(t)P_{1,z}(t) \\
\dot{P}_{1,z}(t) &= \gamma_{In}(t)P_{0,z}(t) - \gamma_{Out}(t)P_{1,z}(t)
\end{aligned}
\tag{8}
$$

with rates $\gamma_{In}(t)$ and $\gamma_{Out}(t)$ for tunneling in and tunneling out, respectively. The factor z in the second term of the upper equation is referred to as the counting variable. We solve these differential equations for a square-function time dependence of the rates. To account for the limited time resolution of the detector, we discretize the differential equations with time steps of length t_{bin} according to ref. 59. The sum $P_z(t) := P_{0,z}(t) + P_{1,z}(t)$ of the results $P_{0,z}(t)$ and $P_{1,z}(t)$ is the z-transform of the distribution $P_N(t)$, which yields the generating function

$$
S_F(z, t) = \ln P_z(t).
\tag{9}
$$

To calculate the factorial cumulants for an interval of lengths Δt, we set $t = t_0 + \Delta t$, average the distribution P_z for fixed Δt over the initial times t_0, take the logarithm and, then, apply Eq. (3). A more detailed description of the theoretical modeling is given in supplementary note 7.

Data availability

The data that support the findings of this study are available from the corresponding author upon reasonable request.

References

1. Benzi, R., Sutera, A. & Vulpiani, A. The mechanism of stochastic resonance. *J. Phys. A: Math. Gen.* **14**, L453–L457 (1981).
2. Gammaitoni, L., Hänggi, P., Jung, P. & Marchesoni, F. Stochastic resonance. *Rev. Mod. Phys.* **70**, 223–287 (1998).
3. Wellens, T., Shatokhin, V. & Buchleitner, A. Stochastic resonance. *Rep. Prog. Phys.* **67**, 45–105 (2004).
4. Benzi, R., Parisi, G., Sutera, A. & Vulpiani, A. Stochastic resonance in climatic change. *Tellus* **34**, 10–16 (1982).
5. Chialvo, D. R. & Apkarian, A. V. Modulated noisy biological dynamics: Three examples. *J. Stat. Phys.* **70**, 375–391 (1993).
6. Douglass, J. K., Wilkens, L., Pantazelou, E. & Moss, F. Noise enhancement of information transfer in crayfish mechanoreceptors by stochastic resonance. *Nature* **365**, 337–340 (1993).
7. Longtin, A., Bulsara, A. & Moss, F. Time-interval sequences in bistable systems and the noise-induced transmission of information by sensory neurons. *Phys. Rev. Lett.* **67**, 656–659 (1991).
8. Zhai, Z.-M., Kong, L.-W. & Lai, Y.-C. Emergence of a resonance in machine learning. *Phys. Rev. Res.* **5**, 033127 (2023).
9. Löfstedt, R. & Coppersmith, S. N. Stochastic resonance: Nonperturbative calculation of power spectra and residence-time distributions. *Phys. Rev. E* **49**, 4821–4831 (1994).
10. Löfstedt, R. & Coppersmith, S. N. Quantum stochastic resonance. *Phys. Rev. Lett.* **72**, 1947–1950 (1994).
11. Grifoni, M., Hartmann, L., Berchtold, S. & Hänggi, P. Quantum tunneling and stochastic resonance. *Phys. Rev. E* **53**, 5890–5898 (1996).
12. Grifoni, M. & Hänggi, P. Coherent and incoherent quantum stochastic resonance. *Phys. Rev. Lett.* **76**, 1611–1614 (1996).
13. Makarov, M. N. Stochastic resonance and nonlinear response in double-quantum-well structures. *Phys. Rev. B* **52**, R2257–R2260 (1995).
14. Thorwart, M. & Jung, P. Dynamical hysteresis in bistable quantum systems. *Phys. Rev. Lett.* **78**, 2503–2506 (1997).
15. Buchleitner, A. & Mantegna, R. N. Quantum stochastic resonance in a micromaser. *Phys. Rev. Lett.* **80**, 3932–3935 (1998).
16. Huelga, S. F. & Plenio, M. B. Stochastic resonance phenomena in quantum many-body systems. *Phys. Rev. Lett.* **98**, 170601 (2007).
17. Singh, K. P. & Rost, J. M. Optimal stochastic enhancement of photoionization. *Phys. Rev. Lett.* **98**, 160201 (2007).
18. Viola, L., Fortunato, E. M., Lloyd, S., Tseng, C. & Cory, D. G. Stochastic resonance and nonlinear response using NMR spectroscopy. *Phys. Rev. Lett.* **84**, 5466–5469 (2000).
19. Wagner, T. et al. Quantum stochastic resonance in an a.c.-driven single-electron quantum dot. *Nat. Phys.* **15**, 330–334 (2019).
20. Hänze, M. et al. Quantum stochastic resonance of individual Fe atoms. *Sci. Adv.* **7**, eabg2616 (2021).
21. Muller, A. et al. Resonance fluorescence from a coherently driven semiconductor quantum dot in a cavity. *Phys. Rev. Lett.* **99**, 187402 (2007).
22. Melet, R. et al. Resonant excitonic emission of a single quantum dot in the Rabi regime. *Phys. Rev. B* **78**, 073301 (2008).
23. Ates, S. et al. Post-selected indistinguishable photons from the resonance fluorescence of a single quantum dot in a microcavity. *Phys. Rev. Lett.* **103**, 167402 (2009).
24. Flagg, E. B. et al. Resonantly driven coherent oscillations in a solid-state quantum emitter. *Nat. Phys.* **5**, 203–207 (2009).
25. Kurzmann, A. et al. Optical blocking of electron tunneling into a single self-assembled quantum dot. *Phys. Rev. Lett.* **117**, 017401 (2016).
26. Hanschke, L. et al. Origin of antibunching in resonance fluorescence. *Phys. Rev. Lett.* **125**, 170402 (2020).
27. Vamivakas, A. N. et al. Observation of spin-dependent quantum jumps via quantum dot resonance fluorescence. *Nature* **467**, 297–300 (2010).
28. Kurzmann, A. et al. Optical detection of single-electron tunneling into a semiconductor quantum dot. *Phys. Rev. Lett.* **122**, 247403 (2019).
29. Lochner, P. et al. Real-time detection of single Auger recombination events in a self-assembled quantum dot. *Nano Lett.* **20**, 1631–1636 (2020).
30. Yilmaz, S. T. et al. Quantum-Dot-Spin Single-Photon Interface. A. *Phys. Rev. Lett.* **105**, 033601 (2010).
31. Appel, M. H. et al. Coherent spin-photon interface with waveguide induced cycling transitions. *Phys. Rev. Lett.* **126**, 013602 (2021).
32. de Greve, K. et al. Quantum-dot spin-photon entanglement via frequency downconversion to telecom wavelength. *Nature* **491**, 421–425 (2012).
33. Kimble, H. J. The quantum internet. *Nature* **453**, 1023–1030 (2008).
34. Wehner, S., Elkouss, D. & Hanson, R. Quantum internet: A vision for the road ahead. *Science* **362**, eaam9288 (2018).
35. Lochner, P. et al. Contrast of 83% in reflection measurements on a single quantum dot. *Sci. Rep.* **9**, 8817 (2019).
36. Vamivakas, A. N., Zhao, Y., Lu, C.-Y. & Atatüre, M. Spin-resolved quantum-dot resonance fluorescence. *Nat. Phys.* **5**, 198–202 (2009).

37. Houel, J. et al. Probing single-charge fluctuations at a GaAs/AlAs interface using laser spectroscopy on a nearby InGaAs quantum dot. *Phys. Rev. Lett.* **108**, 107401 (2012).

38. Matthiesen, C. et al. Phase-locked indistinguishable photons with synthesized waveforms from a solid-state source. *Nat. Commun.* **4**, 1600 (2013).

39. Kuhlmann, A. V. et al. Charge noise and spin noise in a semiconductor quantum device. *Nat. Phys.* **9**, 570–575 (2013).

40. Kerski, J. et al. Post-processing of real-time quantum event measurements for an optimal bandwidth. *Sci. Rep.* **13**, 1105 (2023).

41. Gammon, D., Snow, E. S., Shanabrook, B. V., Katzer, D. S. & Park, D. Fine structure splitting in the optical spectra of single GaAs quantum dots. *Phys. Rev. Lett.* **76**, 3005–3008 (1996).

42. Bayer, M. et al. Fine structure of neutral and charged excitons in self-assembled In(Ga)As/(Al)GaAs quantum dots. *Phys. Rev. B* **65**, 195315 (2002).

43. Zöllner, M. et al. The interplay between electron tunneling and Auger emission in a single quantum emitter weakly coupled to an electron reservoir. *Appl. Phys. Lett.* **124**, 023102 (2024).

44. Hershfield, S., Davies, J. H., Hyldgaard, P., Stanton, C. J. & Wilkins, J. W. Zero-frequency current noise for the double-tunnel-junction Coulomb blockade. *Phy. Rev. B* **47**, 1967–1979 (1993).

45. Blanter, Y. & Büttiker, M. Shot noise in mesoscopic conductors. *Phys. Rep.* **336**, 1–166 (2000).

46. Bagrets, D. A. & Nazarov, Y. V. Full counting statistics of charge transfer in Coulomb blockade systems. *Phy. Rev. B* **67**, 085316 (2003).

47. Gustavsson, S. et al. Counting statistics of single electron transport in a quantum dot. *Phys. Rev. Lett.* **96**, 076605 (2006).

48. Garreis, R. et al. Counting statistics of single electron transport in bilayer graphene quantum dots. *Phys. Rev. Res.* **5**, 013042 (2023).

49. Hussein, R., Kohler, S., Bayer, J. C., Wagner, T. & Haug, R. J. Spectral properties of stochastic resonance in quantum transport. *Phys. Rev. Lett.* **125**, 206801 (2020).

50. Gustavsson, S. et al. Measurements of higher-order noise correlations in a quantum dot with a finite bandwidth detector. *Phys. Rev. B* **75**, 075314 (2007).

51. Flindt, C. et al. Universal oscillations in counting statistics. *PNAS* **106**, 10116–10119 (2009).

52. Komijani, Y. et al. Counting statistics of hole transfer in a p-type GaAs quantum dot with dense excitation spectrum. *Phys. Rev. B* **88**, 035417 (2013).

53. Beenakker, C. W. & Schomerus, H. Counting statistics of photons produced by electronic shot noise. *Phys. Rev. Lett.* **86**, 700–703 (2001).

54. Johnson, N. L., Kemp, A. W. & Kotz, S. *Univariate discrete distributions*. Wiley series in probability and statistics (Wiley-Interscience, Hoboken, N.J, 2005).

55. Kambly, D., Flindt, C. & Büttiker, M. Factorial cumulants reveal interactions in counting statistics. *Phys. Rev. B* **83**, 075432 (2011).

56. Stegmann, P., Sothmann, B., Hucht, A. & König, J. Detection of interactions via generalized factorial cumulants in systems in and out of equilibrium. *Phys. Rev. B* **92**, 592 (2015).

57. Stegmann, P. & König, J. Short-time counting statistics of charge transfer in Coulomb-blockade systems. *Phys. Rev. B* **94**, 125433 (2016).

58. Brange, F., Menczel, P. & Flindt, C. Photon counting statistics of a microwave cavity. *Phys. Rev. B* **99**, 085418 (2019).

59. Kleinherbers, E. et al. Pushing the limits in real-time measurements of quantum dynamics. *Phys. Rev. Lett.* **128**, 087701 (2022).

60. Kleinherbers, E. et al. Unraveling spin dynamics from charge fluctuations. *Phys. Rev. Res.* **5**, 043103 (2023).

61. Mandel, L. Sub-Poissonian photon statistics in resonance fluorescence. *Opt. Lett.* **4**, 205–207 (1979).

62. Talkner, P. Statistics of entrance times. *Physica A* **325**, 124–135 (2003).

63. Talkner, P., Machura, Ł., Schindler, M., Hänggi, P. & Łuczka, J. Statistics of transition times, phase diffusion and synchronization in periodically driven bistable systems. *New J. Phys.* **7**, 14 (2005).

Acknowledgements

Author contributions

H.M., M.Z., N.S., F.R. carried out the experiments on resonance fluorescence. J.Z., E.K. and J.K. developed the theory and analysed the data by full counting statistics. H.M., A.Lo and M.G. designed the experiments and analysed the data. A.Lu. and A.D.W designed and grew the sample. J.Z., H.M., A.Lo., J.K., M.G. wrote the manuscript. All authors contributed to the discussion of the results and the preparation of the manuscript.

Funding

Competing interests

The authors declare no competing interests.

Additional information

Supplementary information The online version contains supplementary material available at https://doi.org/10.1038/s42005-025-02334-4.

Correspondence and requests for materials should be addressed to H. Mannel.

Peer review information *Communications Physics* thanks Christian Flindt and the other, anonymous, reviewers for their contribution to the peer review of this work.

Reprints and permissions information is available at http://www.nature.com/reprints

Publisher's note Springer Nature remains neutral with regard to jurisdictional claims in published maps and institutional affiliations.